Hindawi
Advances in Polymer Technology
Volume 2020, Article ID 8620431, 17 pages
https://doi.org/10.1155/2020/8620431

Research Article

Oxidized Renewable Materials for the Removal of Cobalt(II) and Copper(II) from Aqueous Solution Using in Batch and Fixed-Bed Column Adsorption

Josilene Aparecida Vieira Rodrigues, Luide Rodrigo Martins, Laís Milagres Furtado, Amália Luísa Pedrosa Xavier, Francine Tatiane Rezende de Almeida, Ana Luísa da Silva Lage Moreira, Tânia Márcia Sacramento Melo, Laurent Frédéric Gil, and Leandro Vinícius Alves Gurgel

Departamento de Química, Instituto de Ciências Exatas e Biológicas, Universidade Federal de Ouro Preto, Campus Universitário Morro do Cruzeiro, S/no, Bauxita, 35400-000 Ouro Preto, Minas Gerais, Brazil

Correspondence should be addressed to Leandro Vinícius Alves Gurgel; legurgel@ufop.edu.br

Received 10 June 2019; Revised 7 August 2019; Accepted 16 September 2019; Published 10 January 2020

Academic Editor: Khalid Z. Elwakeel

Batch and continuous adsorption of Co^{2+} and Cu^{2+} from aqueous solutions by oxidized sugarcane bagasse (SBox) and oxidized cellulose (Cox) were investigated. The oxidation reaction of sugarcane bagasse and cellulose was made with a mixture of H_3PO_4–$NaNO_2$ to obtain SBox and Cox, with the introduction of high number of carboxylic acid functions, 4.5 and 4.8 mmol/g, respectively. The adsorption kinetics of Co^{2+} and Cu^{2+} on SBox and Cox were modeled using two models (pseudo-first-order and pseudo-second-order) and the rate-limiting step controlling the adsorption was evaluated by Boyd and intraparticle diffusion models. The Sips and Langmuir models better fitted the isotherms with values of maximum adsorption capacity (Q_{max}) of 0.68 and 0.37 mmol/g for Co^{2+} and 1.20 and 0.57 mmol/g for Cu^{2+} adsorption on Cox and SBox, respectively. The reuse of both spent adsorbents was evaluated. Adsorption of Cu^{2+} and Co^{2+} on SBox in continuous was evaluated using a 2^2 factorial design with spatial time and initial metal concentration as independent variables and Q_{max} and effective use of the bed as responses. The breakthrough curves were very well described by the Bohart–Adams original model and the Q_{max} values for Co^{2+} and Cu^{2+} were 0.22 and 0.55 mmol/g. SBox confirmed to be a promising biomaterial for application on a large scale.

1. Introduction

The pollution of water resources by toxic metal species is one of the main environmental problems in the world. These inorganic pollutants can cause serious negative effects on the ecosystem, because they have high toxicity to living organisms and are persistent in the environment due to their nonbiodegradability. Metal ions such as $Cu^{2+}$and Co^{2+} are essential, but become toxic by excess exposure. Cobalt is an essential element of vitamin B12, which is necessary for the red blood cell production, but becomes toxic [1] when a high amount is ingested by humans, producing an erythropoietic effect, cardiomyopathy, hypothyroidism, and polycythemia. On the other band, the immoderate accumulation of copper in the human body can produce hepatic necrosis and Wilson's disease, resulting in abnormalities of the nervous system, liver, kidneys, and cornea [2, 3].

Nowadays, several processes have been used to remove inorganic pollutants of different sources from water. These processes are mostly conventional processes based on physicochemical treatments (in combination or not) such as coagulation, flocculation, precipitation, and nano- and ultra-filtration [4, 5]. However, these processes have a high cost and/or a low efficiency in removing metal ions at low concentrations and, in addition, some of them can generate a large amount of waste that requires to be further disposed of [6]. Therefore, these problems have increased the number of studies in this area, aimed at the development of original

processes with a higher efficiency and lower cost [7]. In this context, adsorption has been highlighted with the development of new adsorbent materials of lower cost and can be efficiently reused; these materials were obtained from designed syntheses using agroindustrial residues as natural materials [8]. During the two last decades, low-cost bioadsorbents such as lignocellulose biomass [9, 10] from agricultural crop waste or chitosan [11–13] from fishing industry waste have been studied as potential materials to be used in the treatment of effluents containing organic pollutants or toxic metal species.

The reuse of agroindustrial residues adds a greater economic value and mitigates a series of environmental problems caused by them. Agroindustrial residues mainly consist of lignocellulose biomass (LB), which can be applied in the adsorption of toxic metal species as an alternative to conventional adsorbents as activated carbons and styrene-divinylbenzene ion-exchange resins, since agroindustrial residues are cheap and efficient metal ion accumulators [14]. However, LB can be chemically modified to increase their attraction towards specific pollutants or to be applied to specific processes, enhancing their physicochemical properties, such as adsorption capacity, chemical resistance to acidic and basic media, and selectivity [15, 16].

Oxidation process is an interesting strategy to modify chemically LB. In addition, the type of oxidizing mixture used will determine the changes in the chemical groups, physical structure, and crystallinity of the LB, producing oxidized materials with different physicochemical properties [17]. Thus, materials with new interesting properties for many purposes can be obtained [18].

Most previous studies using agroindustrial residues for adsorption of toxic metal species are based on batch equilibrium and kinetic studies. Batch adsorption is useful to provide information about the efficiency of an adsorbent and its physicochemical properties; however, batch adsorption may not be the most convenient process to be applied to an industrial scale that requires the treatment of high flow rates. In this way, for a full-scale adsorption process, continuous adsorption is often preferred [19].

In this study, sugarcane bagasse (SB) and cellulose (Cel) were chemically modified by oxidation with a mixture of sodium nitrite ($NaNO_2$) and orthophosphoric acid (H_3PO_4) to obtain oxidized sugarcane bagasse (SBox) and oxidized cellulose (Cox). Adsorption capacity of SBox and Cox for Co^{2+} and Cu^{2+} ions from spiked aqueous solutions was investigated. The batch adsorption was carried out as a function of the contact time, solution pH and initial Co^{2+} or Cu^{2+} concentration. The reuse of SBox and Cox was also evaluated. The adsorption of Co^{2+} and Cu^{2+} in continuous using a fixed-bed column filled with SBox was evaluated with a 2^2 experimental design.

2. Material and Methods

2.1. Material. Cellulose grade chromatography paper (3MM, Cat. No. 3030–861) was acquired from Whatman, England. Sugarcane bagasse was collected from the Jatiboca Ethanol and Sugar Plant, Urucânia, Minas Gerais, Brazil. HCl (37 wt.% in water), NaOH, HNO_3, H_3PO_4 (85 wt.%), and $CuSO_4{\cdot}5H_2O$ were acquired from Synth (Brazil). $CoCl_2{\cdot}6H_2O$ and $NaNO_2$ were acquired from Vetec (Brazil).

2.2. Cellulose and Sugarcane Bagasse Preparation. An analytical mill (Model A11, IKA) was used to mill 50 mm^2 paper sheets of Cel before oxidation reaction. For oxidation reaction, sugarcane bagasse (SB) was treated using the methodology described by Ramos et al. [20]. The SB fraction utilized in this study was that retained on the 0.150 mm (100 mesh) sieve.

2.3. Oxidation of Sugarcane Bagasse and Cellulose. The oxidation reaction of SB and Cel was performed using the procedure previously described by Martins et al. [21]. In a typical methodology, 5.000 g of Cel or SB was weighed into a 250 mL Erlenmeyer flask and then 80.0 mL of H_3PO_4 (85% wt.%) was added to the flask under agitation at 25°C. Afterward, it was added in this flask 4.000 g of $NaNO_2$ under vigorous agitation for about 10 min and the mixture was allowed to stand for 5 h with the flask opened. Then, a vacuum filtration on a sintered glass funnel (porosity 2) was used to separate the reaction mixture from the oxidized material (SBox or Cox), which was washed with distilled water until pH reached neutrality (pH ~ 7). The drying of the oxidized material was performed in an oven at 65°C for 4 h. The oxidized material was kept in a desiccator prior to use.

2.4. FTIR Spectroscopy. To prepare the FTIR KBr pellets of 13 mm, 100 mg of KBr (spectroscopy grade) and 1 mg of sample (dried powder) were mixed and pressed using a hydraulic press (Model 181-1110, Pike Technologies, Canada) at 6 ton for 30 s. The spectrum was obtained from an FTIR spectrometer (Model MB3000, ABB Bomen, Canada) from 500 to 4000 cm^{-1} with a resolution of 4 cm^{-1} and 32 scans per sample.

2.5. Adsorption Experiments. The adsorption of Cu^{2+} and Co^{2+} on SBox or Cox was studied as a function of the contact time, solution pH, and initial Cu^{2+} or Co^{2+} concentration. The following typical methodology was used in all adsorption experiments, which were carried out in duplicate. Samples of 20 mg of SBox or Cox and 100.0 mL of aqueous Cu^{2+} or Co^{2+} solution were added to 250 mL Erlenmeyer flasks. Then, drops of aqueous 0.1 mol/L NaOH or HCl solutions were added to adjust the pH. The flasks were placed in an orbital incubator shaker (Model TE-424, Tecnal, Brazil) at 150 rpm and 25°C. At the end of the adsorption experiments, a single filtration (filter paper JP-41) was carried out to separate the liquid and solid fractions. A flame atomic absorption spectrophotometer (FAAS) (Model SpectrAA 50B, Varian) was used to determine the concentration of Cu^{2+} or Co^{2+} in the liquid fraction ($\lambda_{Cu} = 324.8$ nm [22], $\lambda_{Co} = 240.7$ nm [22]). The adsorption capacity, q, was calculated utilizing Equation (1):

$$q/(\text{mmol/g}) = \frac{(C_i - C)V}{w}, \tag{1}$$

where $q\,(\text{mmol/g})$ is the amount of Cu^{2+} or Co^{2+} adsorbed per unit weight of SBox or Cox at time t or equilibrium, V (L) is the volume of Cu^{2+} or Co^{2+} solution, C_i (mmol/L) is the initial

Cu^{2+} or Co^{2+} concentration, C (mmol/L) is the Cu^{2+} or Co^{2+} concentration at time t or equilibrium and w (g) is the weight of SBox or Cox.

2.5.1. Adsorption of Cu^{2+} and Co^{2+} on SBox or Cox as a Function of Solution pH. The following conditions were employed to evaluate the effect of solution pH on the adsorption capacity of Cu^{2+} and Co^{2+} on SBox or Cox: pH from 2.0 to 5.5, contact time of 4 h and initial Cu^{2+} or Co^{2+} concentration of 50 mg/L.

2.5.2. Adsorption of Cu^{2+} or Co^{2+} on SBox or Cox as a Function of Contact Time. The following conditions were employed to evaluate the effect of contact time on the adsorption capacity of Cu^{2+} and Co^{2+} on SBox or Cox: time interval from 5 to 600 min, pH 5.5 and initial Cu^{2+} or Co^{2+} concentration of 50 mg/L.

2.5.3. Adsorption of Cu^{2+} or Co^{2+} on SBox or Cox as a Function of Cu^{2+} or Co^{2+} Concentration. The adsorption isotherms were obtained to evaluate the influence of initial Cu^{2+} or Co^{2+} concentration on metal ion uptake by SBox and Cox by varying the initial Cu^{2+} or Co^{2+} concentration. The following conditions were employed to obtain the adsorption isotherms: initial Cu^{2+} or Co^{2+} concentration range from 8 to 100 mg/L, equilibrium time of 3 h and pH 5.5.

2.6. Desorption and Reuse of SBox and Cox. Desorption of SBox and Cox was made to evaluate the possible reuse of these adsorbent materials. The loading of SBox or Cox (50 mg) with Cu^{2+} or Co^{2+} was performed at pH 5.5 using 100.0 mL of 125 mg/L of Cu^{2+} or Co^{2+} solution and a time of 3 h. At the end of adsorption experiments, a single filtration was made to recover the loaded adsorbent, which was washed with distilled water to eliminate any nonadsorbed Cu^{2+} or Co^{2+}. The loaded adsorbent was dried at 80°C in an oven for 1 h. Then, 20 mg of Cox or SBox loaded with Cu^{2+} or Co^{2+} was weighed into Erlenmeyer flasks (125 mL) and then 20.0 mL of aqueous 0.5 mol/L HNO_3 solution was added. Desorption experiments were performed in an orbital incubator shaker (Model TE-424, Tecnal, Brazil) at 150 rpm and 25°C for time intervals of 10 and 15 min for SBox and Cox, respectively. The concentration of Cu^{2+} or Co^{2+} in the desorption solution was determined by FAAS (Section 2.5). The desorption efficiency, E_{des}, was calculated utilizing Equation (2), [17]:

$$E_{\text{des}}/(\%) = \left(\frac{C_e V}{Q_{T,\max} w'_{\text{ads}}}\right) \times 100, \tag{2}$$

where C_e (mg/L) is the equilibrium Cu^{2+} or Co^{2+} concentration in aqueous HNO_3 solution, V (L) is the volume of the aqueous HNO_3 solution, $Q_{T,\max}$ (mg/g) is the maximum adsorption capacity obtained from loading adsorbent with Cu^{2+} or Co^{2+} before the desorption experiment and $w'_{\text{ads}}(g)$ is the weight of SBox or Cox adsorbent contained in SBox or Cox loaded with Cu^{2+} or $Co^{2+}(w_{\text{ads, M}^{2+}})$ [22]. The calculation of w'_{ads} is given in Equation (3):

$$w'_{\text{ads}}/(\text{g}) = \frac{w_{\text{ads, M}^{2+}}}{(Q_{T,\max}/1000) + 1}. \tag{3}$$

All reuse studies were made using the following procedure: 20 mg of SBox or Cox recovered from Cu^{2+} or Co^{2+} desorption was added to Erlenmeyer flasks (250 mL) with 100.0 mL of an aqueous 50 mg/L Cu^{2+} or Co^{2+} solution (pH 5.5). The Erlenmeyer flasks were placed in an orbital incubator shaker (Model TE-424, Tecnal) at 150 rpm and 25°C for 3 h. Then, a single filtration (filter paper JP-41) was used to separate the liquid and solid fractions and the equilibrium concentration of Cu^{2+} or Co^{2+} in the liquid fraction was determined by FAAS (Section 2.5). The re-adsorption efficiency, $E_{\text{re-ads}}$, for one adsorption/desorption/re-adsorption cycle was calculated utilizing Equation (4).

$$E_{\text{re-ads}}/(\%) = \left(\frac{Q_{\text{re-ads, max}}}{Q_{T,\max}}\right) \times 100, \tag{4}$$

where $Q_{\text{re-ads,max}}$ (mg/g) is the maximum re-adsorption capacity obtained after one adsorption/desorption/adsorption cycle [22]. $Q_{\text{re-ads, max}}$ is calculated utilizing Equation (5).

$$Q_{\text{re-ads, max}}/(\text{mg/g}) = \frac{[(w_{\text{ads, M}^{2+}} - w'_{ads})(1 - E_{\text{des}}/100)] - [(C_i - C_e)V]}{w'_{\text{ads}}}. \tag{5}$$

2.7. Fixed-Bed Column Adsorption Experiments. The adsorption experiments in continuous were carried out in a jacket glass column (10.0 cm height × 1.0 cm inner diameter) filled with 0.400 g of SBox adsorbent (dry-weight basis). The SBox adsorbent was packed between two layers containing glass beads (10 mm of diameter) and glass wool to give a uniform upflow of the Cu^{2+} or Co^{2+} solution into the column. For all experiments, the bed height was fixed at 3.80 cm. The inlet upflow rate was controlled by a peristaltic pump (Model BP600/2, Milan, Brazil). The temperature of the inlet metal solution and the column was kept at 25 ± 1°C by a thermostatic bath with forced water circulation (Model MA470, Marconi, Brazil). The Cu^{2+} or Co^{2+} solutions were prepared using a buffer of pH 5.5 (CH_3COOH/CH_3COONa). Effluent samples were sampled at the top of the column at predetermined time intervals to obtain the breakthrough curve. Metal concentration in the effluent samples was determined by FAAS (Section 2.5). To ensure that metal concentration was in the range of the calibration curve, appropriate dilutions were made. The saturation time and breakthrough point were fixed at 95% and 5% of influent metal concentration, respectively [23].

2.7.1. Design of Experiments. The continuous monocomponent adsorption of Cu^{2+} and Co^{2+} on SBox was optimized employing a 2^2 experimental design to evaluate the influence of the initial Cu^{2+} or Co^{2+} concentration (C_0, mmol/L) and spatial time (τ, min) on the responses. The value of τ was calculated using the empty volume of the column (mL) and the flow rate (mL/min). The dependent variables (responses) evaluated were the maximum adsorption capacity ($Q_{\max}$, mmol/g) of the bed and the effective use of the bed (H, cm).

Table 1 presents the independent variables (IVs) and their levels used in the continuous adsorption of Cu^{2+} and Co^{2+} on SBox adsorbent. They were defined considering the batch

Table 1: Independent variables evaluated in the 2^2 experimental design and their levels for Cu^{2+} and Co^{2+} adsorption in a fixed-bed column using SBox as adsorbent.

Independent variable	Level		
	−1	0	+1
$C_0\left(\text{mmol Cu}^{2+}/\text{L}\right)$	0.47	0.86	1.26
$C_0\left(\text{mmol Co}^{2+}/\text{L}\right)$	0.17	0.42	0.68
$\tau(\text{min})$	0.70	1.05	1.40

adsorption studies and the lowest flow rate (1.4 mL/min) of the pump. Then, 1 min was defined as the center point of spatial time; and the center point of initial Cu^{2+} and Co^{2+} concentration was calculated based on the values of C_e obtained from the batch adsorption isotherms.

Statistica 10.0 (StatSoft, Inc.) routines were used to evaluate the obtained results for analyses of variance (ANOVA), regression coefficients and graphical analysis. To analyze the experimental error, pure error was used and a confidence level equal to 95% was used in the statistical analyses. An *IV* was statistically significant when its p-value <0.05.

2.8. Modeling the Experimental Data

2.8.1. Batch Kinetic Data. Pseudo-first-order (PFO) and pseudo-second-order (PSO) models were used to investigate the adsorption kinetics of Cu^{2+} and Co^{2+} on SBox and Cox.

The PFO kinetic model of Lagergren [24] is expressed by Equation (6).

$$q_t/(\text{mmol/g}) = q_e\left[1 - \exp\left(-k_1 t\right)\right], \tag{6}$$

where $k_1\left(\text{min}^{-1}\right)$ is the pseudo-first-order rate constant.

The PSO kinetic model of Ho and McKay [25] is expressed by Equation (7).

$$q_t/(\text{mmol/g}) = \frac{k_2 q_e^2 t}{1 + k_2 q_e t}, \tag{7}$$

where $k_2\left(\text{g/mmol min}\right)$ is the pseudo-second-order rate constant.

In addition, to elucidate the adsorption mechanism of Cu^{2+} and Co^{2+} on Cox and SBox, two models were used: intraparticle diffusion (IPD) and Boyd.

The IPD model of Weber and Morris [26] is expressed by Equation (8).

$$q_t/(\text{mmol/g}) = k_i t^{1/2} + C, \tag{8}$$

where $C\left(\text{mmol/g}\right)$ is the intercept and $k_i\left(\text{mmol/g min}^{1/2}\right)$ is the intraparticle diffusion rate constant. The constant C may be correlated to the thickness of the boundary layer.

The model of Boyd et al. [27] is expressed by Equation (9):

$$f = 1 - \frac{6}{\pi^2}\sum_{n=1}^{\infty}\frac{1}{n^2}\exp\left(-n^2 B_t\right), \tag{9}$$

where $f\left(f = q_t/q_e\right)$ is the fractional surface coverage as a function of time and B_t is a function of f. Reichenberg [28] provided solutions for Equation (9) using Fourier transform, which are expressed by Equations (10) and (11), as follows:

$$B_t = -0.4977 - \ln(1 - f), \tag{10}$$

$$B_t = \left(\sqrt{\pi} - \sqrt{\pi - \frac{\pi^2 f}{3}}\right)^2. \tag{11}$$

For $f > 0.85$, Equation (10) was utilized, whereas for $f < 0.85$, Equation (11) was utilized to obtain the values of B_t.

The effective diffusion coefficient, D_i, was determined by Equation (12), as follows:

$$D_i/\left(m^2/\text{min}\right) = \frac{Br^2}{\pi^2}, \tag{12}$$

where r is the radius of the Cox ($r = 0.250 \times 10^{-3}$ m) or SBox ($r = 0.150 \times 10^{-3}$ m) particles, assuming a spherical shape.

2.8.2. Batch Equilibrium Data. Adsorption isotherms were fitted by the Freundlich, Langmuir, and Sips isotherm models.

The Langmuir [29] isotherm model is expressed by Equation (13).

$$q_e/(\text{mmol/g}) = \frac{Q_{\max} b C_e}{1 + bC_e}, \tag{13}$$

where $Q_{\max}\left(\text{mmol/g}\right)$ is the maximum adsorption capacity of SBox or Cox for a metal ion and $b\,(\text{L/mmol})$ is the Langmuir binding constant.

The Freundlich [30] isotherm model is expressed by Equation (14).

$$q_e/(\text{mmol/g}) = K_F C_e^{1/n}, \tag{14}$$

where $K_F\left[\text{mmol/g}\,(\text{L/mmol})^{1/n}\right]$ and n are the Freundlich model constants. The parameter n is associated to the adsorption intensity.

The Langmuir–Freundlich isotherm model, developed by Sips [31], is a hybrid model of the Freundlich and Langmuir isotherm models, which is expressed by Equation (15).

$$q_e/(\text{mmol/g}) = Q_{\max}\frac{\left(bC_e\right)^{1/n}}{1 + \left(bC_e\right)^{1/n}}, \tag{15}$$

where n is a parameter describing the heterogeneity of the system.

2.8.3. Analysis of the Breakthrough Curve. The area under the breakthrough curves gives the amount of Cu^{2+} or Co^{2+} adsorbed in the bed [32]. Then, the value of $Q_{\max}$ of the bed can be obtained from Equation (16), until the saturation time $\left(t_s\right)$ is reached, as follows:

$$Q_{\max}/(\text{mmol/g}) = \frac{C_0 \dot{V}}{1000 w_{\text{SBox}}}\int_0^t\left(1 - \frac{C_t}{C_0}\right)dt, \tag{16}$$

where $\dot{V}$ is the inlet flow rate (mL/min), t is the time, C_0 and C_t are the influent and effluent Cu^{2+} or Co^{2+} concentrations (mmol/L) and w_{SBox} is the weight of SBox (g).

The value of H is defined as the height of the bed that was effectively utilized in the continuous adsorption process [33]. The value of H was obtained from Equation (17), as follows:

$$H/\text{cm} = \left(\frac{q_{M^{2+},t_b}}{q_{M^{2+},t_s}}\right)Z, \tag{17}$$

where Z is the bed height (cm), q_{M^{2+},t_b} is the amount of Cu^{2+} or Co^{2+} adsorbed on the adsorbent until the breakthrough time (t_b) (mmol) and q_{M^{2+},t_s} is the amount of Cu^{2+} or Co^{2+} adsorbed on the adsorbent until the saturation time (t_s) (mmol). The values of q_{M^{2+},t_b} and q_{M^{2+},t_s} were determined by the integration of the area under the breakthrough curves until t_b and t_s, respectively.

(i) Modeling the Breakthrough Curves. The development of mathematical models to predict the breakthrough curve, the mechanism involved in the process and even the evaluation of the effect of different variables on adsorption process is an important demand. However, this is a difficult task for such systems since the concentration profiles in both solid and liquid phases vary with both Z and t [32]. Thus, analytical models based on modeling the experimental data by means of nonlinear or linear regression analyses with physical meaning are available [34–38]. The original model of Bohart and Adams [38] is successfully employed when the adsorption isotherm is favorable. This model supposes that the rate of adsorption is proportional to the remaining adsorption capacity of the adsorbent and the concentration of the solute, neglecting axial dispersion. Equations (18)–(20) describe the relationship between C_t/C_0 and t for this model.

$$\frac{C_t}{C_0} = \frac{\exp(\alpha)}{\exp(\alpha) + \exp(\beta) - 1}, \tag{18}$$

$$\alpha = k_{\text{B-A}}C_0\left(t - \frac{Z}{\nu}\right), \tag{19}$$

$$\beta = \frac{k_{\text{B-A}}\rho_b Q_{\max} Z}{\nu\varepsilon}, \tag{20}$$

where ν (cm/min) is the interstitial velocity, C (mmol/L) is the liquid phase Cu^{2+} or Co^{2+} concentration initially (C_0) and at time $t(C_t)$, Z (cm) is the column height, t (min) is the time, ε is the column void fraction, ρ_b (g/mL) is the bulk density and $k_{\text{B-A}}$ (L/mmol min) is the Bohart–Adams kinetic rate constant.

The relation between the adsorbent density (ρ_p) and bulk density (ρ_b) was used to determine the porosity of the bed, as given in Equation (21).

$$\varepsilon = 1 - \frac{\rho_b}{\rho_p}. \tag{21}$$

2.8.4. Calculation of Variation in Standard Free Energy of Adsorption. The variation in standard free energy of adsorption $(\Delta_{\text{ads}}G^\circ)$ for batch adsorption was determined by Equation (22) [39].

$$\Delta_{\text{ads}}G^\circ/(\text{kJ}/mol) = -RT\ln K_a, \tag{22}$$

where $T(K)$ is the absolute temperature, K_a is the thermodynamic equilibrium constant (dimensionless) and R is the gas constant (8.3144 J/K mol).

Liu [39] suggested that b (Langmuir constant) can be used to calculate the value of K_a, as given in Equation (23).

$$K_a = \left[\frac{b}{\gamma_e}(1\ \text{mol}/L)\right], \tag{23}$$

where γ_e is the activity coefficient (dimensionless) at equilibrium at 25°C.

The value of γ_e can be calculated utilizing the extended Debye Hückel law (Equation (24)), which is applied to ionic strengths up to 0.1 mol/L.

$$\log\gamma_e = \frac{-0.509z^2\sqrt{I_e}}{1 + (\alpha\sqrt{I_e}/305)}, \tag{24}$$

where I_e (mol/L) is the ionic strength, z is the charge of the Cu^{2+} or Co^{2+} and α (pm) is the hydrated ion size of Cu^{2+} or Co^{2+} (600 pm) [40]. The values of I_e were calculated as described by Ramos et al. [20].

2.8.5. Regression Analysis and Error Evaluation.

(i) Batch Adsorption Data. The experimental batch equilibrium and kinetic data were modeled with the PFO and PSO and Freundlich, Langmuir, and Sips models by nonlinear regression (NLR) analysis using Microcal OriginPro®2015. The modeling of the kinetic data with IPD and Boyd models was made by linear regression (LR) analysis of the experimental data. The software was set to use the weight method named "statistical" and the Levenberg–Marquardt algorithm. The reduced chi-square (χ^2_{red}) was employed to determine which model best described the experimental adsorption data [41].

(ii) Continuous Adsorption Data. The breakthrough curves obtained were fitted using the set of Equations (18)–(20). The algorithm genetic function (ga) of the MATLAB®2010a software (Mathworks Inc.) was used for adjusting the parameters of the Bohart-Adams model to the continuous experimental data by minimization of the objective function. The objective function used was the root-mean-square error (RMSE) [18], as given in Equation (25).

$$\text{RMSE} = \sqrt{\frac{\sum_{i=1}^{n}(y_i - \hat{y}_i)^2}{n}}, \tag{25}$$

where n is the number of experimental points and y_i is the value of experimental point i, $\hat{y}_i$ is the predicted value by the model for the experimental point i.

3. Results and Discussion

3.1. Synthesis and Characterization of the Oxidized Materials. The oxidation reaction of SB and Cel was performed using a mixture of $NaNO_2$ and H_3PO_4 to obtain the adsorbent materials SBox and Cox with high amounts of

carboxylic acid groups according to the optimized procedure reported in a previous study by our research group [21]. The use of this oxidation system (H_3PO_4-$NaNO_2$) provides a cheaper methodology to prepare materials containing carboxyl functionality, thus adding value to these materials. The reaction mainly produced the oxidation of the primary R-CH_2OH groups of SB and Cel into R-COOH groups. The reaction conditions were optimized by response surface methodology (RSM) and design of experiments (DOE). Through the optimization of the synthesis conditions, SBox and Cox were obtained with a number of R-COOH functions (n_{COOH}) of 4.5 and 4.8 mmol/g, respectively, which were determined as described by Martins et al. [21]. Cel oxidation was accomplished with a weight gain equal to 7.7%. This can be explained by the fact that the primary alcohol groups were converted into carboxylic acid groups, increasing the molar mass of the biopolymer. A weight loss equal to 18.4% was reported for SB oxidation, because of the presence of oxidant species and the acidic conditions, which degraded lignin and hemicelluloses fractions, increasing the solubility of these fractions in an aqueous medium.

SBox and Cox were characterized by FTIR spectroscopy and solid-state ^{13}C NMR spectroscopy, as described in our previous study by Martins et al. [21]. The ^{13}C NMR spectrum of Cox indicated that the main product has carboxylic acid groups but that starting material (nonoxidized cellulose) is also still present in much smaller amounts.

The main advantage of these oxidized materials (SBox and Cox) comparing to other carboxylated materials prepared by our research group [14, 15, 20, 22, 42–45] is that carboxylic acid functions in SBox and Cox are mainly from the oxidation of primary hydroxyl groups (R-CH_2OH) of cellulose (in SB or Cel). On the contrary, when carboxylic acid groups are introduced in the Cel or SB through esterification reaction with cyclic carboxylic acid anhydrides, the application of esterified Cel or SB is limited to a pH range where the ester groups may not be easily hydrolyzed in the aqueous phase, e.g., 2–9 [46].

3.2. Adsorption Studies

3.2.1. Effect of Solution pH on the Removal of Cu^{2+} and Co^{2+} by SBox and Cox. The batch removal of Cu^{2+} and Co^{2+} by adsorption on SBox and Cox from spiked aqueous solutions depends on the solution pH, since both adsorbent materials contain ionizable carboxylic acid groups. The net surface charge of the adsorbents in aqueous solution is directly related to pH of point of zero charge (pH_{PZC}). The values of pH_{PZC} for SBox and Cox are 2.72 and 2.70, respectively, as reported by Martins et al. [21]. Thus, at pH values greater than pH_{PZC} both surfaces of SBox and Cox became predominantly negative due to conversion of carboxylic acid groups into carboxylate anion. Therefore, when pH values are higher than 2.7, SBox and Cox have a net negative surface charge, thereby promoting the adsorption of the cationic pollutants, such as Cu^{2+} and Co^{2+}.

Graphs of q_e against initial solution pH for adsorption of Cu^{2+} and Co^{2+} on Cox and SBox are shown in Figures 1(a) and 1(b), respectively. As expected, the adsorption of both metals increased when the solution pH was higher, reaching a maximum at pH value of 5.5 for all adsorption systems. Interestingly, Cox exhibited a higher q_e value than SBox for both metals studied, with both adsorbent materials even having a similar value for n_{COOH}. Then, the next studies of adsorption of Cu^{2+} and Co^{2+} on both materials as a function of the contact time (kinetics) and initial Cu^{2+} and Co^{2+} concentration (isotherm) were carried out at a pH value of 5.5.

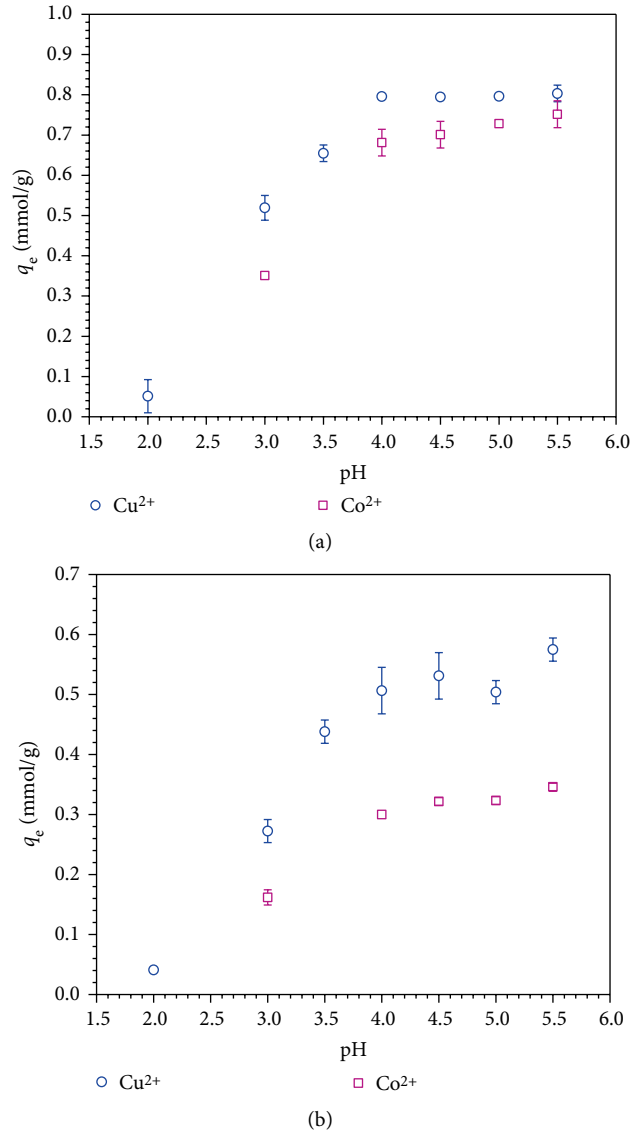

Figure 1: Effect of initial solution pH on the adsorption of Co^{2+} and Cu^{2+} on (a) Cox and (b) SBox (contact time of 4 h, 0.79 mmol/L Cu^{2+}, 0.85 mmol/L Co^{2+}, 25°C, 150 rpm, 0.2 g/L Cox or SBox).

A similar tendency was reported by Gurgel et al. [14, 43] and Ramos et al. [20] for the adsorption of Cu^{2+} on succinylated cellulose (Cell 6) [14], succinylated sugarcane bagasse (SCB 2) [43] and sugarcane bagasse modified with trimellitic anhydride (STA) [20]. SCB 2 has a higher amount of carboxylic acid groups (6.0 mmol/g), but a higher pH_{PZC} value (5.26) [47] than SBox [21]. As a result, SCB 2 only exhibited an adsorptive capacity for Cu^{2+} ions from a pH value of 3.0. The pH_{PZC} value of STA is 3.16 because this material possesses

carboxylic acid groups bonded to an aromatic ring and showed more significant adsorptive capacity for Cu^{2+} and Co^{2+} ions from a pH value of 3.0. In the present study, because of the structural properties of SBox and Cox, i.e. a carboxyl group directly bonded to the glycosyl ring, both SBox and Cox are able to adsorb Cu^{2+} ions from a pH of 2.0 due to their lower pH_{PZC} values. This represents a great advantage of SBox and Cox in comparison to other carboxylated materials prepared from lignocellulose biomass that have been reported in the literature.

3.2.2. Effect of Contact Time on the Removal of Cu^{2+} and Co^{2+} by SBox and Cox. To design a wastewater treatment plant operating in batch or continuous mode, it is fundamental to study and understand the adsorption kinetics. Thus, experiments with each metal and SBox and Cox adsorbents were performed to define the values of q_e and equilibrium time (t_e) as well as the adsorption rate constant. Other important factors to explain the adsorption mechanism are the physicochemical and textural properties of the Cox and SBox adsorbents as well as the mass transport processes.

The curves generated from the NLR analyses of the experimental data with the PFO and PSO are presented in Figures 2(a) and 2(b). Table 2 presents kinetic parameters estimated by modeling of the experimental data. Comparing the values of R^2 and χ^2_{red} presented in Table 2, it was possible to confirm that the PSO model better described the Cu^{2+} adsorption by both adsorbent materials. When comparing the values of $q_{e,exp}$ of Cu^{2+} with those of $q_{e,est}$, it can be observed for both adsorbent materials that the values of $q_{e,est}$ estimated by the PSO model were closer to those of $q_{e,exp}$.

The values of k_2 indicated a higher kinetic rate constant for Cu^{2+} adsorption on SBox than Cox. As can be seen in Figures 2(a) and 2(b), the equilibrium time for Cu^{2+} adsorption was achieved in 45 and 120 min for SBox and Cox, respectively.

For Co^{2+} adsorption on both SBox and Cox, the model that better described the experimental data was the PFO model with the values of $q_{e,exp}$ for this model being closer to those values of $q_{e,est}$. The values of k_1 showed a higher kinetic rate constant for Co^{2+} adsorption on Cox than SBox. As can be seen in Figures 2(a) and 2(b), the Co^{2+} adsorption equilibrium time was achieved in 180 and 120 min for SBox and Cox, respectively.

The parameters of IPD and Boyd models estimated by LR analyses of the experimental data are presented in Table 2. The adsorption process of Cu^{2+} and Co^{2+} on SBox and Cox exhibited three stages (Figures not shown). These plots suggest that the adsorption of Cu^{2+} and Co^{2+} on SBox and Cox was initially governed by the diffusion of Cu^{2+} or Co^{2+} through the thin solvent film surrounding both Cox and SBox particles and then changed to intraparticle diffusion. Afterward, equilibrium was reached. Boyd's plots (Figures not shown) were only linear for the initial stage of Cu^{2+} or Co^{2+} adsorption and did not intersect the origin, suggesting that external mass transfer can be the rate-limiting step governing the initial stage of Cu^{2+} or Co^{2+} adsorption, which then changed to intraparticle diffusion, corroborating the IPD plots [48]. In addition, for both adsorbent materials, the values of D_i were higher for Cu^{2+} adsorption than Co^{2+} adsorption, which will have a great influence in the behavior of Cu^{2+} and Co^{2+} adsorption on SBox in a fixed-bed column, as presented in Section 3.4.

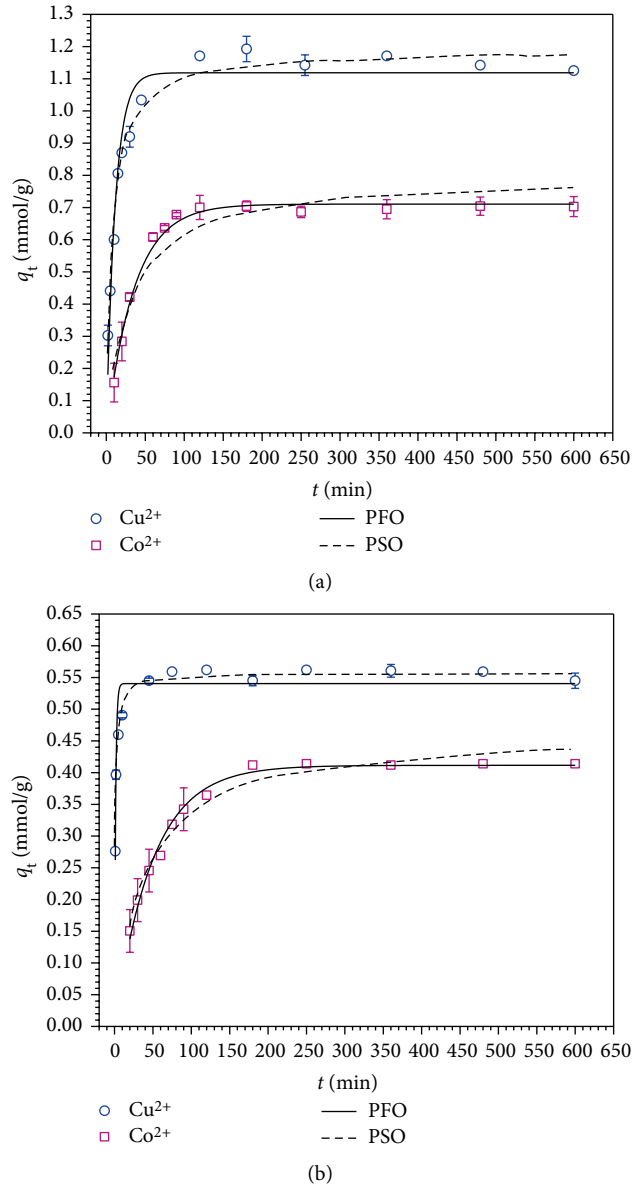

FIGURE 2: Effect of contact time on the adsorption of Cu^{2+} and Co^{2+} on (a) Cox and (b) SBox (25°C, 150 rpm, pH 5.5, 0.79 mmol/L Cu^{2+}, 0.85 mmol/L Co^{2+}, 0.2 g/L Cox or SBox).

3.2.3. Adsorption Isotherms of Cu^{2+} and Co^{2+} on SBox and Cox. Adsorption isotherms can be employed to describe the different affinities of various solutes for the adsorption sites of an adsorbent. To evaluate the equilibrium data, Freundlich, Langmuir, and Sips models, three of various isotherm models available in the literature, were chosen. The isotherm model parameters estimated by fitting the models to the experimental data are presented in Table 3. The curves fitted to the

Table 2: Results of modeling the experimental kinetic data for the adsorption of Cu^{2+} and Co^{2+} on Cox and SBox (25°C, 150 rpm, pH 5.5, 0.79 mmol/L Cu^{2+}, 0.85 mmol/L Co^{2+}, 0.2 g/L Cox or SBox).

Parameter	Cox-Cu^{2+}	Cox-Co^{2+}	SBox-Cu^{2+}	SBox-Co^{2+}
$q_{e,exp}$ (mmol/g)	1.16 ± 0.02	0.70 ± 0.01	0.56 ± 0.01	0.41 ± 0.02
$q_{e,exp}$ (mg/g)	73.53 ± 1.58	41.18 ± 0.41	35.30 ± 0.52	23.87 ± 1.17
t_e (min)	120	120	45	180
Model		*Pseudo-first-order (PFO)*		
$q_{e,est}$ (mmol/g)	1.12 ± 0.04	0.71 ± 0.01	0.54 ± 0.01	0.41 ± 0.01
$q_{e,est}$ (mg/g)	71.08 ± 2.28	41.88 ± 0.58	34.33 ± 0.63	24.25 ± 0.34
k_1 (min^{-1})	0.088 ± 0.010	0.028 ± 0.001	0.664 ± 0.064	0.020 ± 0.001
R^2	0.952	0.994	0.930	0.989
R^2_{adj}	0.947	0.993	0.923	0.988
χ^2_{red}	0.008	8.44×10^{-4}	0.002	4.14×10^{-4}
Model		*Pseudo-second-order (PSO)*		
$q_{e,est}$ (mmol/g)	1.19 ± 0.02	0.80 ± 0.04	0.56 ± 0.00	0.47 ± 0.01
$q_{e,est}$ (mg/g)	75.42 ± 1.50	47.11 ± 2.12	35.37 ± 0.27	27.41 ± 0.65
k_2 (g/mmol min)	0.109 ± 0.011	0.042 ± 0.008	1.865 ± 0.110	0.055 ± 0.006
R^2	0.984	0.955	0.988	0.981
R^2_{adj}	0.983	0.950	0.987	0.979
χ^2_{red}	0.003	0.006	2.87×10^{-4}	7.42×10^{-4}
Model		*Intraparticle diffusion (IPD)*		
1st step				
(mmol/g $min^{1/2}$)	0.171 ± 0.001	0.114 ± 0.011	0.291 ± 0.000	0.036 ± 0.004
(mmol/g)	0.061 ± 0.003	−0.210 ± 0.050	−0.015 ± 0.000	−0.006 ± 0.023
R^2	0.999	0.991	1.000	0.980
R^2_{adj}	0.999	0.981	—	0.969
2nd step				
(mmol/g $min^{1/2}$)	0.077 ± 0.007	0.040±	0.033 ± 0.000	0.019 ± 0.004
(mmol/g)	0.512 ± 0.036	0.296±	0.385 ± 0.00	0.153 ± 0.035
R^2	0.985	0.983	1.000	0.967
R^2_{adj}	0.977	0.966	—	0.934
Model		*Boyd*		
B	0.035 ± 0.003	0.031 ± 0.002	0.135 ± 0.034	0.016 ± 0.000
Intercept	0.030 ± 0.057	−0.403 ± 0.116	0.380 ± 0.193	−0.213 ± 0.060
D_i (m^2/min)	2.19×10^{-10}	1.98×10^{-10}	8.55×10^{-10}	9.98×10^{-11}
R^2	0.974	0.983	0.888	0.986
R^2_{adj}	0.969	0.978	0.832	0.983

experimental data of Cu^{2+} and Co^{2+} adsorption on SBox and Cox are presented in Figures 3(a) and 3(b).

The isotherm curves obtained presented a downward-concave profile, characterizing a favorable adsorption [35]. The steepest initial slopes of adsorption isotherms of Cu^{2+} on SBox and Cox in comparison to Co^{2+} adsorption isotherms on SBox and Cox indicate that Cu^{2+} ions had more affinity for the adsorption sites of SBox and Cox than Co^{2+} ions. This is corroborated by the higher values of b for Cu^{2+} adsorption than for Co^{2+} adsorption (Table 3). In addition, for both Cu^{2+} and Co^{2+}, even at low metal concentrations, the adsorbed amount was relatively high until reaching a plateau at which the adsorbed amount remained constant. In agreement with the classification of isotherms proposed by Giles et al. [49], the profiles of the isotherm curves for all adsorption systems studied corresponded to group L, subgroup 2.

The adsorption isotherms (Figures 3(a) and 3(b)) with initial curvature (type L) suggest that the available active sites are more difficult to find when the surface coverage increases, indicating that the Cu^{2+} and Co^{2+} may have been adsorbed onto a monolayer.

The evaluation of the values of χ^2_{red} and the comparison between the values of $Q_{max,exp}$ and $Q_{max,est}$ were used to select the best isotherm model in order to characterize the adsorption systems. Analyzing the values of χ^2_{red}, $Q_{max,exp}$ and $Q_{max,est}$ presented in Table 3, it can be seen that for Cu^{2+} or Co^{2+} adsorption on both adsorbents, both the Sips and Langmuir isotherm models can describe very well the experimental data. The Sips model is a hybrid of the Freundlich and Langmuir isotherms. The parameter n of the Sips model can be employed to evaluate the degree of heterogeneity of an adsorption system. Thus, if the value of n is closer to unity, this suggests a

Table 3: Isotherm model parameters estimated for the adsorption of Cu^{2+} and Co^{2+} on Cox and SBox (pH 5.5, 25°C, 150 rpm and 0.2 g/L Cox or SBox).

Isotherm model	Parameter	Cox-Cu^{2+}	Cox-Co^{2+}	SBox-Cu^{2+}	SBox-Co^{2+}
Experimental data	$Q_{max,exp}$ (mmol/g)	1.20 ± 0.01	0.68 ± 0.01	0.57 ± 0.00	0.37 ± 0.00
	$Q_{max,exp}$ (mg/g)	76.14 ± 0.92	39.82 ± 0.33	36.23 ± 0.10	22.05 ± 0.25
	I_e (mol/L)	3.145×10^{-3}	3.365×10^{-3}	3.148×10^{-3}	3.407×10^{-3}
	γ_e	0.789	0.783	0.789	0.782
	CN	4.01	7.10	7.89	12.03
Langmuir	$Q_{max,est}$ (mmol/g)	1.17 ± 0.03	0.70 ± 0.01	0.60 ± 0.01	0.40 ± 0.00
	$Q_{max,est}$ (mg/g)	74.36 ± 2.11	41.24 ± 0.35	38.07 ± 0.57	23.64 ± 0.22
	b (L/mmol)	30.47 ± 0.068	23.04 ± 1.09	17.93 ± 1.24	11.67 ± 0.53
	R^2	0.914	0.988	0.977	0.989
	R^2_{adj}	0.908	0.987	0.974	0.988
	χ^2_{red}	0.006	2.08×10^{-4}	4.40×10^{-4}	1.03×10^{-4}
	K_a	38616.6	29430.3	22728.9	14944.3
	ΔG° (kJ/mol)	−26.18	−25.51	−24.87	−23.83
Freundlich	K_F [(mmol/g)(L/mmol)$^{1/n}$]	1.22 ± 0.02	0.68 ± 0.01	0.57 ± 0.01	0.37 ± 0.01
	n	5.43 ± 0.26	7.25 ± 0.78	6.01 ± 0.52	5.39 ± 0.43
	$1/n$	0.184	0.138	0.167	0.185
	R^2	0.975	0.900	0.933	0.939
	R^2_{adj}	0.974	0.890	0.926	0.933
	χ^2_{red}	0.002	0.002	0.001	5.89×10^{-4}
Sips	$Q_{max,est}$ (mmol/g)	1.62 ± 0.08	0.72 ± 0.01	0.64 ± 0.03	0.42 ± 0.01
	$Q_{max,est}$ (mg/g)	102.83 ± 5.01	42.52 ± 0.77	40.68 ± 1.59	25.01 ± 0.62
	b (L/mmol)	10.71 ± 2.54	23.88 ± 1.17	17.20 ± 1.53	11.26 ± 0.58
	n	2.26 ± 0.15	1.19 ± 0.10	1.37 ± 0.18	1.24 ± 0.10
	R^2	0.997	0.992	0.988	0.995
	R^2_{adj}	0.996	0.991	0.986	0.993
	χ^2_{red}	2.27×10^{-4}	1.45×10^{-4}	2.47×10^{-4}	5.73×10^{-5}

more homogeneous adsorption; and if the value of n is equal to unity, the Sips isotherm is reduced to the Langmuir isotherm. Contrarily, if the value of n is far from unity, this indicates a more heterogeneous adsorption system, approaching to the Freundlich model.

From the values of n reported in Table 3 for the Sips model, it is concluded that the adsorption systems involving the adsorption of Co^{2+} on SBox and Cox are more homogeneous than the adsorption systems involving the adsorption of Cu^{2+} on SBox and Cox. It is also noted that the adsorption of Cu^{2+} on Cox is significantly more heterogeneous than other adsorption systems studied.

Parameter b of the Langmuir model is associated to the solute affinity for the adsorbent sites [50]. Comparing the values of b of the Langmuir model (Table 3), it is concluded that Cu^{2+} has a greater affinity for both Cox and SBox adsorption sites than Co^{2+}, as was previously concluded by the initial slopes of Cu^{2+} adsorption isotherms in comparison to Co^{2+} adsorption isotherms. The solute affinity for the adsorbent sites of the materials increased in the order: Co^{2+}-SBox < Cu^{2+}-SBox < Co^{2+}-Cox < Cu^{2+}-Cox.

The values of variation in standard free energy of adsorption ($\Delta_{ads}G^\circ$) were negative for all adsorption systems studied, indicating the spontaneous character of the adsorption in the standard conditions. Adsorption experiments of Cu^{2+} on raw cellulose (Cel) and raw sugarcane bagasse (SB) were only performed for comparison purposes. The values of Q_{max} for Cu^{2+} adsorption on SB and Cel were 0.23 mmol/g (13.3 mg/g) and 0.21 mmol/g (13.2 mg/g), respectively, which showed that SBox and Cox presented a much higher Q_{max} than SB and Cel. For, example, the values of $Q_{max,exp}$ for Cu^{2+} adsorption on SBox and Cox were 2.7 times and 5.8 times higher than SB and Cel, respectively, which shows the efficiency of the functionalization process of SB and Cel to obtain SBox and Cox.

The values of the coordination numbers (CN) (Table 3) [14] for Cu^{2+} and Co^{2+} adsorption on SBox and Cox suggested that not all carboxylic acid groups were available to adsorb metals. The values of CN for adsorption of Cu^{2+} and Co^{2+} on

Table 4: Desorption efficiency (E_{des}) and re-adsorption efficiency ($E_{re\text{-}ads}$) for Cu^{2+} and Co^{2+} for Cox and SBox adsorbents.

Material	Metal ion	E_{des} (%)	$E_{re\text{-}ads}$ (%)
Cox	Cu^{2+}	87.7	99.4
	Co^{2+}	72.3	98.4
SBox	Cu^{2+}	98.1	104.1
	Co^{2+}	85.3	92.9

Cox were lower than those for adsorption on SBox, indicating that the n_{COOH} taking part on the adsorption of Cu^{2+} and Co^{2+} by SBox and Cox was different. Probably, this was responsible for a decrease in the value of Q_{max} for SBox in comparison to Cox, as both Cox (4.8 mmol/g) and SBox (4.5 mmol/g) have similar values for n_{COOH}.

3.3. Desorption and Reuse of SBox and Cox. Desorption and re-adsorption were evaluated for both SBox and Cox adsorbents with Cu^{2+} and Co^{2+}, respectively. The desorption efficiencies (E_{des}) and re-adsorption efficiencies ($E_{re\text{-}ads}$) obtained for both SBox and Cox are presented in Table 4.

It was observed that the desorption of the metals was fast, with a maximum value of E_{des} achieved in a short time, i.e., 10 min for SBox and 15 min for Cox. The best result for E_{des} was obtained for the SBox-Cu system; however, the other systems showed values of E_{des} between 72.3% and 87.7%. Even though SBox and Cox were not completely desorbed, this should not impair their reuse as they still present a large amount of free adsorption sites.

The desorption experiments performed at acidic aqueous medium showed that both metals were fast desorbed, which indicated the ion-exchange was the mechanism controlling both adsorption and desorption of both metals. Xavier et al. [23], who investigated the adsorption/desorption/re-adsorption of Co^{2+}, Cu^{2+} and Ni^{2+} on trimellitated sugarcane bagasse reported a similar behavior in comparison to that observed in the present study.

The infrared spectra of Cox and SBox before and after desorption of Cu^{2+} (Cox-D- Cu^{2+}, SBox-D-Cu^{2+}) and Co^{2+} (Cox-D-Co^{2+}, SBox-D-Co^{2+}), respectively, are presented in Figures 4(a) and 4(b). As can be seen in Figures 4(a) and 4(b), the band at 1730 cm^{-1} related to C=O stretching in carboxylic acid groups is still present in both spectra of Cox and SBox after desorption of Cu^{2+} and Co^{2+}, showing that both adsorbent materials were not degraded after desorption.

Re-adsorption was performed to evaluate the alternative of reusing both adsorbents. The desorbed SBox and Cox were used in a new adsorption cycle to evaluate their performances as they were not completely desorbed. The obtained results are shown in Table 4. The lower value of $E_{re\text{-}ads}$ was for Co^{2+}-SBox system; however, the other systems showed values of $E_{re\text{-}ads}$ higher than >98%. Therefore, SBox and Cox still exhibited excellent values of $E_{re\text{-}ads}$ in comparison to their values of $Q_{T,max}$ showing that these materials are interesting adsorbents from both point of view of chemical resistance to degradation and reuse.

3.4. Monocomponent Adsorption of $Cu^{2+}$and Co^{2+} on SBox Adsorbent in a Fixed-Bed Column. The choice of SBox to investigate continuous adsorption of Cu^{2+} and Co^{2+} in a fixed-bed column is due to its lower cost in comparison to Cox, although Cox had higher values of $Q_{max,exp}$ in comparison to SBox.

The breakthrough curves plotted as effluent concentration-time profiles provide information about the dynamic behavior of a determined fixed-bed column adsorption from the mass transfer zone (MTZ). MTZ is the area of the bed where the adsorption of Cu^{2+} and Co^{2+} occurs. MTZ varies

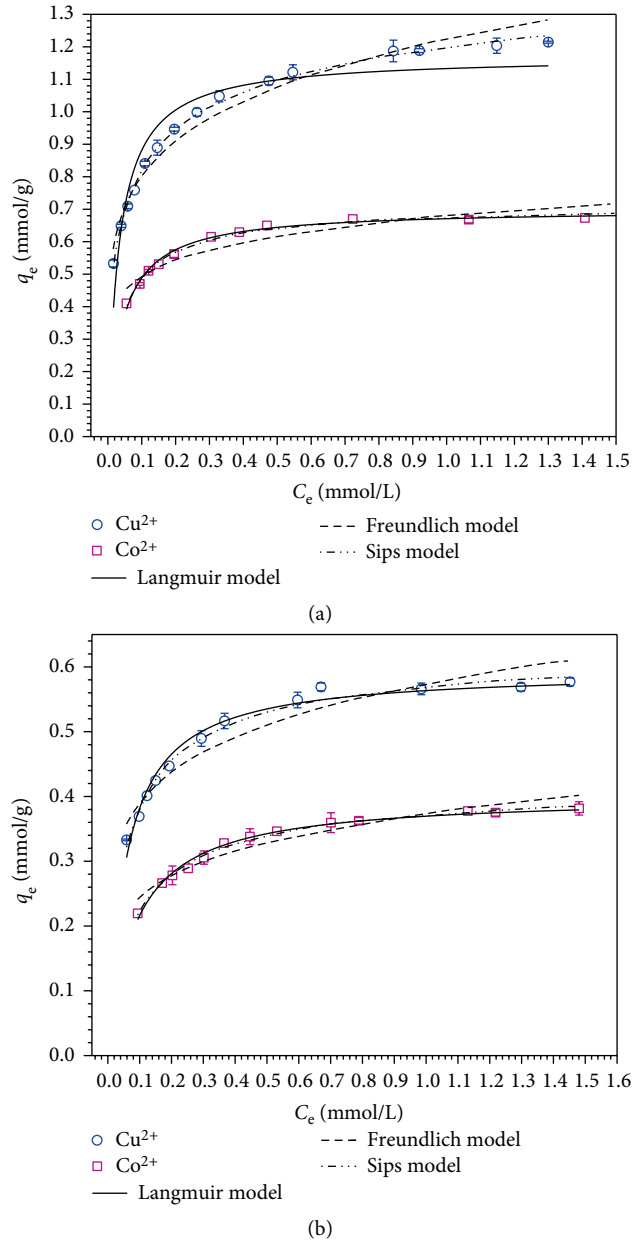

FIGURE 3: Isotherms for adsorption of Cu^{2+} and Co^{2+} on (a) Cox and (b) SBox (pH 5.5, 25°C, 150 rpm, and 0.2 g/L Cox or SBox).

with t_b, which is the time when the value of C in the effluent reaches 5% of C_0, to t_s, which is the time when the value of C in the effluent reaches 95% of C_0. Figures 5(a) and 5(b) present the breakthrough curves obtained for adsorption of Cu^{2+} and Co^{2+} on SBox in a fixed-bed column. Table 5 presents the values of H and Q_{max}.

The results presented in Table 5 show that the higher value of Q_{max} (0.554 mmol/g) for Cu^{2+} adsorption was obtained in experiment 3, while the lower value of Q_{max} (0.237 mmol/g) was obtained in experiment 2. For Co^{2+} adsorption, the higher and lower values of Q_{max} (0.224 and 0.088 mmol/g) were obtained in experiments 3 and 2, respectively. These results suggest that higher levels of initial metal concentration and lower levels of spatial time favored higher values of Q_{max}.

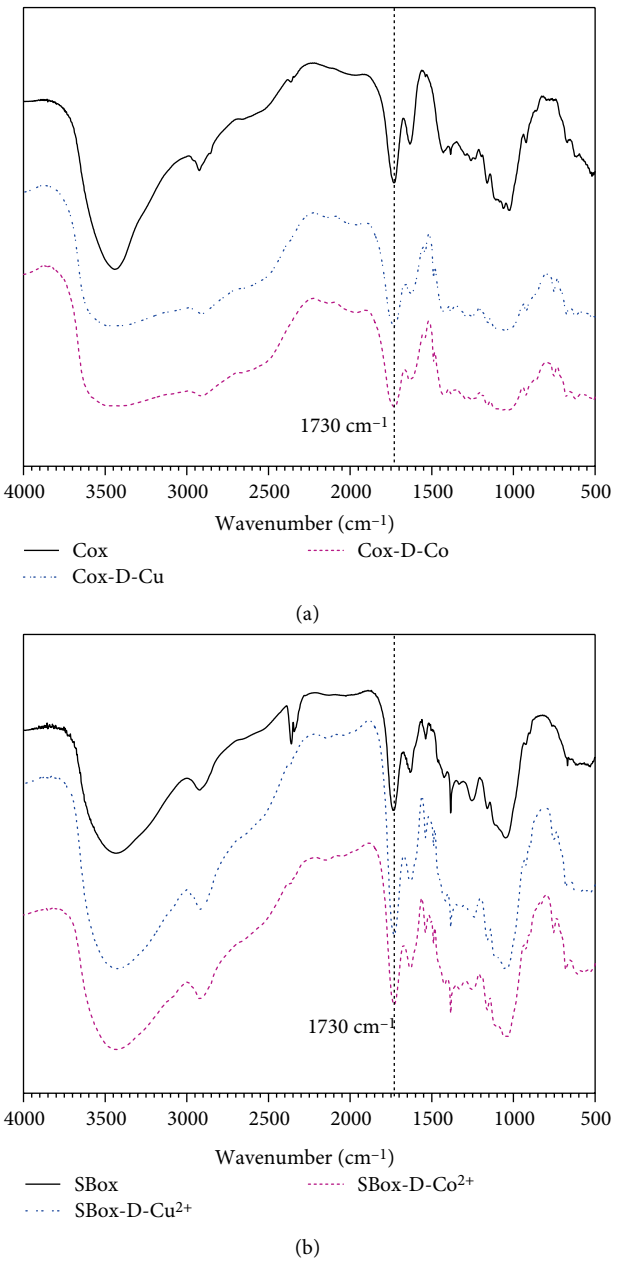

FIGURE 4: FTIR spectra of (a) Cox, Cox-D-Cu^{2+} and Cox-D-Co^{2+} and (b) SBox, SBox-D-Cu^{2+} and SBox-D-Co^{2+}.

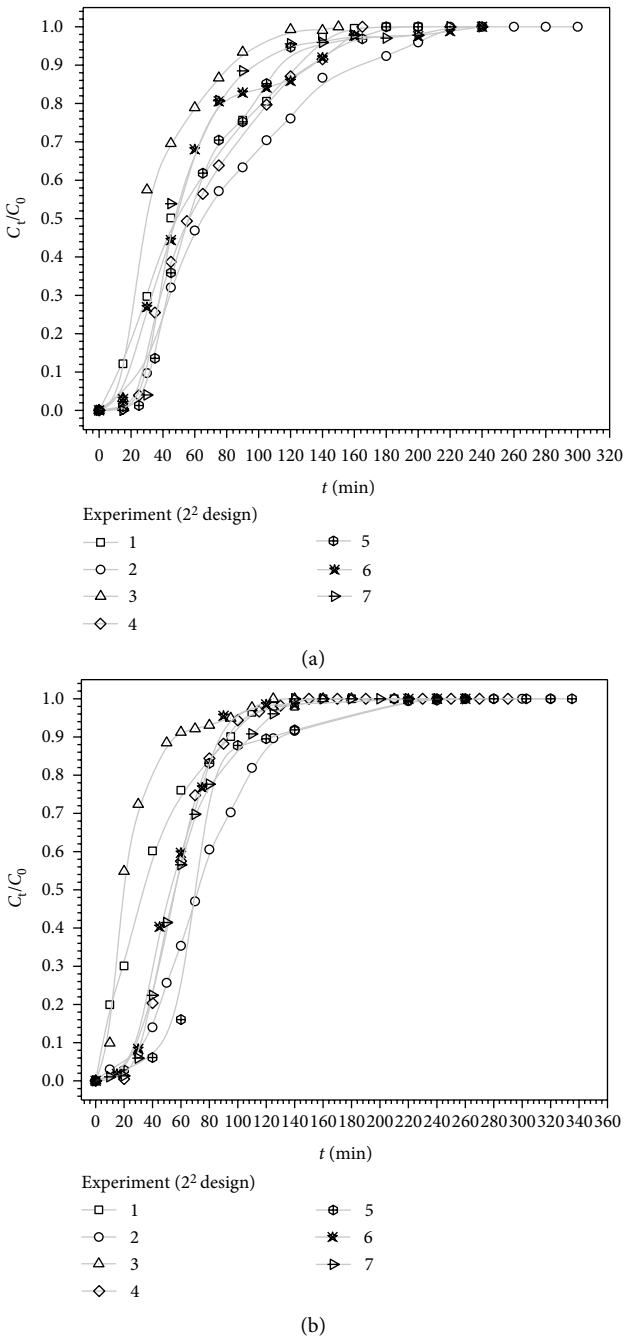

FIGURE 5: Breakthrough curves for adsorption of (a) $Cu^{2+}$and (b) Co^{2+} on SBox adsorbent in a fixed-bed column at 25°C (experiments from 1 to 7 refers to the 2^2 experimental design matrices for Cu^{2+} and Co^{2+} presented in Tables 1 and 5).

Furthermore, lower levels of initial metal concentration and higher levels of spatial time disfavored higher values of Q_{max}. In addition, the value of Q_{max} for Cu^{2+} in continuous adsorption was 2.9% lower than in batch adsorption, while the value of Q_{max} for Co^{2+} in continuous adsorption was 65.2% lower than in batch adsorption.

The rate-limiting steps of an adsorption process are: (1) the mass transfer of the Cu^{2+} or Co^{2+} from the bulk phase to the SBox surface; (2) the diffusion of the Cu^{2+} or Co^{2+} into the SBox porous structure; and (3) the adsorption of Cu^{2+} or Co^{2+} onto the SBox surface [52]. In a mass transfer process, the mass flow is proportional to the concentration gradient difference. This is the driving force for the adsorption process. Moreover, the resistance at the liquid film interface (step 1) decreases with increasing flow rate. Therefore, it is expected that higher levels of inlet Cu^{2+} or Co^{2+} concentration and lower levels of spatial time provide a higher concentration gradient difference between the adsorbed Cu^{2+} or Co^{2+} at the interface and the Cu^{2+} or Co^{2+} in the bulk solution, as well as a smaller resistance at the liquid film, thereby increasing the value of Q_{max} of the adsorbent.

Higher values of H for adsorption of Cu^{2+} and Co^{2+} on SBox were obtained at the center point for both metal ions,

Table 5: Results of 2^2 experimental design for adsorption of Cu^{2+} and Co^{2+} on SBox adsorbent in a fixed-bed column at 25°C.

Number of experiment	Independent variable		Cu^{2+}		Co^{2+}	
	C_0 (mmol/L)	τ (min)	Q_{max} (mmol/g)	H (cm)	Q_{max} (mmol/g)	H (cm)
1	−1	−1	0.261	0.40	0.091	0.23
2	−1	1	0.237	0.73	0.088	0.82
3	1	−1	0.554	1.50	0.224	0.68
4	1	1	0.428	1.41	0.220	1.58
5	0	0	0.316	1.61	0.203	2.12
6	0	0	0.345	1.54	0.195	1.39
7	0	0	0.347	1.67	0.192	1.71

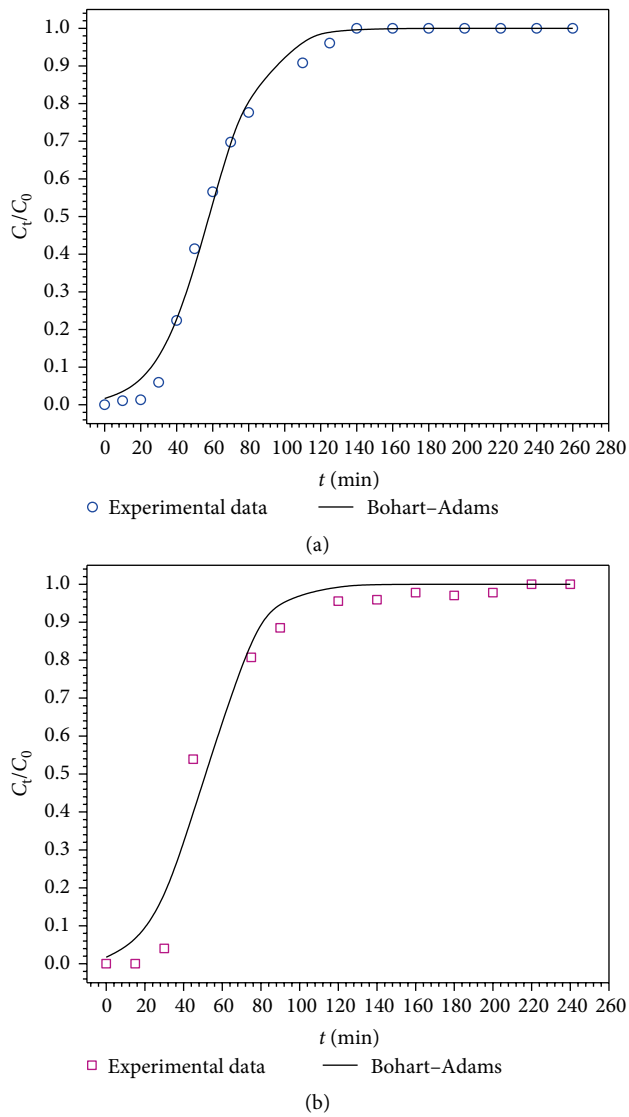

Figure 6: Breakthrough curves for experiment 7 of the 2^2 experimental design modeled by the Bohart-Adams original model for adsorption of (a) Cu^{2+} and (b) Co^{2+} on SBox adsorbent in a fixed-bed column at 25°C.

with 1.67 (experiment 7) and 2.12 cm (experiment 5), respectively. The lower values of H, 0.40 cm for Cu^{2+} and 0.23 cm for Co^{2+}, were obtained in experiment 1. The characteristics of the breakthrough curve are related with the equilibrium adsorption, mass transfer of Cu^{2+} or Co^{2+} from the bulk solution to the SBox surface and porous structure of the SBox as well as with fluid flow properties during continuous adsorption into the column [52]. The instantaneous equilibrium produces, under ideal conditions, a shock-like wave which moves as a sharp concentration step through the bed [53], where the entire length of bed is utilized. This suggests that, at the center point, the overall resistance to the adsorption of Cu^{2+} or Co^{2+} on SBox is reduced, favoring the adsorption. As a consequence, the application of lower levels of C_0 and lower levels of τ increased the overall resistance to the adsorption.

The 2^2 experimental design was employed to evaluate the effect of C_0 and τ on the adsorption of Cu^{2+} and Co^{2+} on SBox in continuous. The analysis of variance (ANOVA) of the experimental data was carried out. The results are shown in Table 6. It is necessary to have a significant regression for a well-adjusted model, i.e., $F > F_{tab}$ and $p < 0.05$ together with a non-significant lack of fit, i.e., $F < F_{tab}$ and $p > 0.05$. The linear model used to fit the response Q_{max} yielded coefficients of determination (R^2) of 0.963 for Cu^{2+} and 0.857 for Co^{2+}. However, the values of R^2 for H for adsorption of Cu^{2+} (0.579) and Co^{2+} (0.358) were not high as for Q_{max}. In addition, the models used to fit the DVs Q_{max} for Co^{2+} and H for Cu^{2+} exhibited a lack of fit, indicating that these models cannot predict the behavior of these dependent variables very well.

As can be seen in Table 6, both independent variables were statistically significant for response Q_{max} for Cu^{2+} with τ presenting a negative effect and C_0 a positive effect on Cu^{2+} adsorption. This means that the use of C_0 in a higher level and τ in a lower level favored a higher value of Q_{max}. The DV Q_{max} for Co^{2+} adsorption was only influenced by C_0 with this variable presenting a statistically significant positive effect. For the DV H, both variables were not statistically significant for Co^{2+} adsorption, and only C_0 was statistically significant, presenting a positive effect on Cu^{2+} adsorption. The interactions between the independent variables $(C_0 \times \tau)$ had no statistically significant effects on any DVs (Q_{max} or H) evaluated for the adsorption of both metals on SBox.

When comparing these results of adsorption in continuous with the profiles of the kinetic curves obtained for batch adsorption of Cu^{2+} and Co^{2+} on SBox (Figures 2(a) and 2(b)), it can be seen that the spatial time only influenced Cu^{2+} adsorption, which presented kinetic curves with steeper initial slopes than those for Co^{2+} adsorption. This suggests that the mass transfer of Cu^{2+} or Co^{2+} from the bulk phase to the SBox surface may have contributed more to the

Table 6: ANOVA for 2^2 experimental design for adsorption of Cu^{2+} and Co^{2+} on SBox in a fixed-bed column adsorption at 25°C.

Response	$Q_{max}Cu^{2+}(R^2 = 0.963)$						$H\,Cu^{2+}(R^2 = 0.579)$					
Factor	Effect	*SS*	*dF*	*MS*	*F*	*p*	Effect	*SS*	*dF*	*MS*	*F*	*p*
(1) τ (min)	−0.075	0.006	1	0.006	18.536	0.050	0.12	0.014	1	0.014	3.402	0.206
(2) C_0 (mmol/L)	0.242	0.058	1	0.058	192.608	0.005	0.890	0.792	1	0.792	187.110	0.005
1 by 2	−0.051	0.003	1	0.003	8.622	0.099	−0.210	0.044	1	0.044	10.417	0.084
Lack of fit		0.002	1	0.002	6.528	0.125		0.610	1	0.610	144.166	0.007
Pure error		0.001	2	0.000				0.008	2	0.004		
Total SS		0.069	6					1.469	6			
Response	$Q_{max}\,Co^{2+}(R^2 = 0.857)$						$H\,Co^{2+}(R^2 = 0.358)$					
Factor	Effect	*SS*	*dF*	*MS*	*F*	*p*	Effect	*SS*	*dF*	*MS*	*F*	*p*
(1) τ/(min)	−0.004	0.000	1	0.000	0.387	0.597	0.745	0.555	1	0.555	4.145	0.179
(2) C_0/(mmol/L)	0.132	0.017	1	0.017	465.534	0.002	0.605	0.366	1	0.366	2.734	0.240
1 by 2	−0.001	0.000	1	0.000	0.011	0.927	0.155	0.024	1	0.024	0.179	0.713
Lack of fit		0.003	1	0.003	75.858	0.013		1.427	1	1.427	10.660	0.082
Pure error		0.000	2	0.000				0.268	2	0.134		
Total SS		0.020	6					2.640	6			

Table 7: Results of the modeling the experimental breakthrough curves with the Bohart–Adams model for adsorption of Cu^{2+} and Co^{2+} on SBox adsorbent in a fixed-bed column at 25°C.

Metal ion	Cu^{2+}						
Number of experiment	1	2	3	4	5	6	7
$Q_{max,exp}$ (mmol/g)	0.261	0.237	0.554	0.428	0.316	0.345	0.347
$k_{B\text{-}A}$/(L/mmol min)	0.101	0.075	0.061	0.042	0.092	0.068	0.100
Q_{max} (mmol/g)	0.249	0.215	0.480	0.377	0.294	0.291	0.288
RMSE	0.053	0.047	0.085	0.066	0.056	0.062	0.065
R^2	0.979	0.979	0.944	0.964	0.980	0.967	0.973
Metal ion	Co^{2+}						
Number of experiment	1	2	3	4	5	6	7
$Q_{max,exp}$ (mmol/g)	0.091	0.088	0.224	0.220	0.203	0.195	0.192
$k_{B\text{-}A}$/(L/mmol min)	0.322	0.253	0.213	0.118	0.158	0.162	0.164
Q_{max}/(mmol/g)	0.081	0.080	0.165	0.204	0.201	0.176	0.171
RMSE	0.043	0.022	0.059	0.019	0.047	0.034	0.032
R^2	0.985	0.997	0.967	0.997	0.986	0.992	0.994

rate-limiting step for Cu^{2+} adsorption on SBox while Co^{2+} adsorption on SBox may be influenced by both diffusional and adsorption rates.

Table 7 presents the results when Bohart-Adams original model was used to model the experimental breakthrough curves. The Bohart-Adams original model better fitted the experimental breakthrough curves for Co^{2+} adsorption than those for Cu^{2+} adsorption, presenting higher R^2 values and smaller RMSE values. The values of Q_{max} estimated by the Bohart-Adams original model and those obtained experimentally presented low values of mean absolute error (*MAE*), between 4.2% and 1.9% for Cu^{2+} and Co^{2+} adsorption, respectively, showing that this model can predict the experimental data very well.

Figures 6(a) and 6(b) show the breakthrough curves obtained for the experiment 7 for adsorption of Cu^{2+} and Co^{2+} on SBox in continuous modeled by the Bohart-Adams original model. The values of Bohart-Adams rate constants ($k_{B\text{-}A}$) for the metals studied were smaller for higher levels of C_0 and/or τ, whereas higher values of $k_{B\text{-}A}$ were observed for lower levels of C_0 and/or τ. The $k_{B\text{-}A}$ is a lumped parameter [51], which includes all effects of internal and external diffusion, adsorption kinetics as well as any dispersion in the bed. Then, the adsorption in continuous at the conditions evaluated in this study is influenced by all of these effects. However, for Cu^{2+} adsorption, the $k_{B\text{-}A}$ value at center point was closer to experiment 1, while for Co^{2+} adsorption in the experiment 4 had a value of $k_{B\text{-}A}$ closer to that obtained at the center point. As the levels of C_0 and τ in experiments 1 and 4 were opposite (Table 5), this indicates that the adsorption of these metals on SBox, in fact, presented different rate-limiting steps.

3.5. Comparison with Literature Adsorption Data for Cu^2 and Co^{2+} on Different Adsorbents. Table 8 presents some adsorbents reported in the literature for the removal of Co^{2+} and Cu^{2+} from spiked aqueous solutions in continuous. It is

Table 8: Comparison of adsorbent materials reported in the literature for removal of Cu^{2+} and Co^{2+} from aqueous solutions in a fixed-bed column adsorption.

Adsorbent	Fixed-bed column adsorption parameter				Q_{max}/(mmol/g)		Fixed-bed model	Reference
	pH	T (°C)	C_0/(mmol/L)	τ/(min)	Cu^{2+}	Co^{2+}		
SBox	5.5	25	1.26 (Cu), 0.68 (Co)	0.7	0.55	0.22	B-A[b]	This study
Tetraethylenepentamine modified sugarcane bagasse	5.0	30-35	0.31	-	0.26	-	-	[55]
Sugarcane bagasse modified with trimellitic anhydride (STA)	5.5	25	0.94 (Cu), 1.61 (Co)	1.05 (Cu); 1.4 (Co)	1.06	0.80	Thomas[a] and B-A[a]	[23]
Citrus maxima peel					1.54	-		
Passion fruit shell	5.4–5.7	25	4.72	1.2	0.57	-	Thomas[a]	[56]
Sugarcane bagasse					0.35	-		
Multi-metal binding biosorbent (MMBB)	5.5	23	0.47	8	0.75	-	Thomas[a]	[57]
Bagasse fly ash (BFA)					0.42	-		
Conventional zeolitic BFA (CZBFA)	5.0	30	3.14	4.3	0.83	-	-	[58]
Electrolyte treated CZBFA					0.84	-		
Magnetized sawdust (Fe_3O_4-SD)	5.0	25	0.16	0.67	0.50	-	Thomas[a] and B-A[a]	[59]
Sargassum wightii biomass	4.5	-	1.70	3.9		0.83	BDST	[60]
Biomass beads of immobilized *Saccharomyces cerevisiae* (PTCC 5010)	8.0	25	1.70	19.6		0.04	Thomas[a]	[61]
Polyamine chelating resin (NDC-984)	5.0	30	5.00	12.0		0.96	-	[62]
Native teak leaves power	-	30	0.85	3.14	-	0.35	Thomas[a] and B-A[a]	[63]
Biochar of teak leaves					-	0.39		
Free seaweed *Sargassum sp.*	5.0	30	0.77	31.4	1.51	-	Thomas[b]	[64]
Immobilized seaweed *Sargassum sp.*			0.78		1.69	-		
Seaweed *Sargassum sp.*	3.5	30	2.08	31.4	0.12	-	Thomas[b] and B-A[b]	[65]

[a]Simplified model; [b]Original model. Thomas: Thomas model; B–A: Bohart–Adams model; BDST: Bed depth service time.

possible to compare the performance of different adsorbent materials in continuous from the values of Q_{max}, C_0, and τ. Both the values of C_0 and τ affect the value of Q_{max} of an adsorbent material. It is possible to have a high value of Q_{max} using a high value of C_0 combined with a low value of τ or a low value of C_0 combined with a high value of τ. Comparing the performance of SBox adsorbent in continuous with those reported in the literature data, it should be noted that SBox showed a very good performance, mainly for Cu^{2+} removal, because it presented a medium value of Q_{max}, which was obtained from a lower value of τ combined with a medium value of C_0. However, SBox presented a lower value of Q_{max} for Co^{2+} removal.

4. Conclusions

The oxidized sugarcane bagasse (SBox) and cellulose (Cox) were successfully synthesized by a cheap chemical modification method and shown to be efficient for the removal of Cu^{2+} and Co^{2+} from spiked single aqueous solutions in both batch and continuous. The adsorption of Cu^{2+} on SBox and Cox was better modeled by the pseudo-second-order kinetic model, while the adsorption of Co^{2+} on SBox and Cox was better modeled by the pseudo-first-order kinetic model. The results of equilibrium adsorption were modeled by three isotherm models and the Sips and Langmuir models closely fitted the experimental data with maximum adsorption capacities (Q_{max}) of 1.20 and 0.57 mmol/g for Cu^{2+} and 0.68 and 0.37 mmol/g for Co^{2+} adsorption on Cox and SBox, respectively. In addition, Cox and SBox exhibited excellent desorption efficiencies (E_{des}) and re-adsorption efficiencies $(E_{re\text{-}ads})$, allowing their reuse in further adsorption cycles. SBox was further used in fixed-bed column adsorption experiments. The Bohart–Adams original model fitted continuous adsorption data very well. The value of Q_{max} for Cu^{2+} (0.55 mmol/g) was closer to batch adsorption, while Q_{max} for Co^{2+} (0.22 mmol/g) was lower than that obtained in batch adsorption. Thus, the main results obtained in this study show that both adsorbents are interesting materials for a real application in a wastewater treatment plant, mainly SBox, which is a cheaper adsorbent in comparison to Cox.

Data Availability

The data used to support the findings of this study are included within the article.

Conflicts of Interest

The authors declare that they have no conflicts of interest.

Acknowledgments

The authors are grateful to Universidade Federal de Ouro Preto (UFOP), Conselho Nacional de Desenvolvimento Científico e Tecnológico (CNPq grant number 448346/2014-1 and CNPq PVE grant number 400739/2014-3) and Fundação de Amparo à Pesquisa do Estado de Minas Gerais (FAPEMIG grant numbers CEX-APQ-01764/14 and CEX-APQ-01287-15) for funding this research. This study was financed in part by the Coordenação de Aperfeiçoamento de Pessoal de Nível Superior - Brasil (CAPES) - Finance Code 001. The authors are also grateful to UFOP (for a master scholarship awarded to J. A. V. Rodrigues).

References

[1] D. J. Paustenbach, B. E. Tvermoes, K. M. Unice, B. L. Finley, and B. D. Kerger, "A review of the health hazards posed by cobalt," *Critical Reviews in Toxicology*, vol. 43, no. 4, pp. 316–362, 2013.

[2] C. G. Fraga, "Relevance, essentiality and toxicity of trace elements in human health," *Molecular Aspects of Medicine*, vol. 26, no. 4–5, pp. 235–244, 2005.

[3] O. Bandmann, K. H. Weiss, and S. G. Kaler, "Wilson's disease and other neurological copper disorders," *The Lancet Neurology*, vol. 14, no. 1, pp. 103–113, 2015.

[4] A. Bandyopadhyay and M. Biswas, "Removal of hexavalent chromium by synergism modified adsorption," *Indian Journal of Environmental Protection*, vol. 18, pp. 662–671, 1998.

[5] G. Crini, "Non conventional low-cost adsorbents for dye removal: a review," *Bioresource Technology*, vol. 97, pp. 1061–1085, 2006.

[6] X. Li, S. Liu, Z. Na, D. Lu, and Z. Liu, "Adsorption, concentration, and recovery of aqueous heavy metal ions with the root powder of *Eichhornia crassipes*," *Ecological Engineering*, vol. 60, pp. 160–166, 2013.

[7] F. Fu and Q. Wang, "Removal of heavy metal ions from wastewaters: a review," *Journal of Environmental Management*, vol. 92, no. 3, pp. 407–418, 2011.

[8] W. S. Wan Ngah and M. A. K. M. Hanafiah, "Removal of heavy metal ions from wastewater by chemically modified plant wastes as adsorbents: a review," *Bioresource Technology*, vol. 99, no. 10, pp. 3935–3948, 2008.

[9] C. Escudero-Oñate, N. Fiol, J. Poch, and I. Villaescusa, "Valorisation of lignocellulosic biomass wastes for the removal of metal ions from aqueous streams: a review," in *Biomass Volume Estimation and Valorization for Energy*, J. S. Tumuluru, Ed., pp. 381–407, InTech, Rijeka, 2017.

[10] M. Vandenbossche, M. Jimenez, M. Casetta, and M. Traisnel, "Remediation of heavy metals by biomolecules: a review," *Critical Reviews in Environmental Science and Technology*, vol. 45, no. 15, pp. 1644–1704, 2014.

[11] K. Z. Elwakeel, A. M. Elgarahy, and S. H. Mohammad, "Magnetic Schiff's base sorbent based on shrimp peels wastes for consummate sorption of chromate," *Water Science and Technology*, vol. 76, no. 1, pp. 35–48, 2017.

[12] K. Z. Elwakeel, A. S. Al-Bogami, and A. M. Elgarahy, "Efficient retention of chromate from industrial wastewater onto a green magnetic polymer based on shrimp peels," *Journal of Polymers and the Environment*, vol. 26, no. 5, pp. 2018–2029, 2018.

[13] K. Z. Elwakeel, M. H. Aly, M. A. El-Howety, E. El-Fadaly, and A. Al-Said, "Synthesis of chitosan@activated carbon beads with abundant amino groups for capture of Cu(II) and Cd(II) from aqueous solutions," *Journal of Polymers and the Environment*, vol. 26, no. 9, pp. 3590–3602, 2018.

[14] L. V. A. Gurgel, O. K. Junior, R. P. D. F. Gil, and L. F. Gil, "Adsorption of Cu(II), Cd(II), and Pb(II) from aqueous single metal solutions by cellulose and mercerized cellulose chemically modified with succinic anhydride," *Bioresource Technology*, vol. 99, no. 8, pp. 3077–3083, 2008.

[15] S. N. C. Ramos, A. L. P. Xavier, F. S. Teodoro, L. F. Gil, and L. V. A. Gurgel, "Removal of cobalt(II), copper(II), and nickel(II) ions from aqueous solutions using phthalate-functionalized sugarcane bagasse: mono- and multicomponent adsorption in batch mode," *Industrial Crops and Products*, vol. 79, pp. 116–130, 2016.

[16] J.-X. Yu, J. Zhu, L.-Y. Feng, and R.-A. Chi, "Simultaneous removal of cationic and anionic dyes by the mixed sorbent of magnetic and non-magnetic modified sugarcane bagasse," *Journal of Colloid and Interface Science*, vol. 451, pp. 153–160, 2015.

[17] A. J. Varma and V. B. Chavan, "A study of crystallinity changes in oxidised celluloses," *Polymer Degradation and Stability*, vol. 49, no. 2, pp. 245–250, 1995.

[18] N. Isobe, X. Chen, U.-J. Kim et al., "TEMPO-oxidized cellulose hydrogel as a high-capacity and reusable heavy metal ion adsorbent," *The Journal of Hazardous Materials*, vol. 260, pp. 195–201, 2013.

[19] K. H. Chu, "Improved fixed bed models for metal biosorption," *Chemical Engineering Journal*, vol. 97, no. 2–3, pp. 233–239, 2004.

[20] S. N. C. Ramos, A. L. P. Xavier, F. S. Teodoro et al., "Modeling mono-and multi-component adsorption of cobalt (II), copper (II), and nickel (II) metal ions from aqueous solution onto a new carboxylated sugarcane bagasse. part I: batch adsorption study," *Industrial Crops and Products*, vol. 74, pp. 357–371, 2015.

[21] L. R. Martins, J. A. V. Rodrigues, O. F. H. Adarme, T. M. S. Melo, L. V. A. Gurgel, and L. F. Gil, "Optimization of cellulose and sugarcane bagasse oxidation: application for adsorptive removal of crystal violet and auramine-O from aqueous solution," *Journal of Colloid and Interface Science*, vol. 494, pp. 223–241, 2017.

[22] F. S. Teodoro, S. N. D. C. Ramos, M. M. C. Elias et al., "Synthesis and application of a new carboxylated cellulose derivative. Part I: removal of Co^{2+}, Cu^{2+} and Ni^{2+} from monocomponent spiked aqueous solution," *Journal of Colloid and Interface Science*, vol. 483, pp. 185–200, 2016.

[23] A. L. P. Xavier, O. F. H. Adarme, L. M. Furtado et al., "Modeling adsorption of copper(II), cobalt(II) and nickel(II) metal ions from aqueous solution onto a new carboxylated sugarcane bagasse. Part II: optimization of monocomponent fixed-bed column adsorption," *Journal of Colloid and Interface Science*, vol. 516, pp. 431–445, 2018.

[24] S. Y. Lagergren, "Zur theorie der sogenannten adsorption gelöster stoffe," *Kungliga Svenska Vetenskapsakademiens, Handlingar*, vol. 24, pp. 1–39, 1898.

[25] Y. S. Ho and G. McKay, "Pseudo-second order model for sorption processes," *Process Biochemistry*, vol. 34, no. 5, pp. 451–465, 1999.

[26] W. J. Weber and J. C. Morris, "Kinetics of adsorption on carbon from solution," *Journal of the Sanitary Engineering Division*, vol. 89, pp. 31–60, 1963.

[27] G. E. Boyd, A. W. Adamson, and L. S. Myers, "The exchange adsorption of ions from aqueous solutions by organic zeolites. II. Kinetics," *Journal of the American Chemical Society*, vol. 69, no. 11, pp. 2836–2848, 1947.

[28] D. Reichenberg, "Properties of ion-exchange resins in relation to their structure. III. Kinetics of exchange," *Journal of the American Chemical Society*, vol. 75, no. 3, pp. 589–597, 1953.

[29] I. Langmuir, "The adsorption of gases on plane surfaces of glass, mica and platinum," *Journal of the American Chemical Society*, vol. 40, no. 9, pp. 1361–1403, 1918.

[30] H. M. Freundlich, "Over the adsorption in solution," *Zeitschrift für Physikalische Chemie*, vol. 57, pp. 385–470, 1906.

[31] R. Sips, "On the structure of a catalyst surface," *Journal of Chemical Physics*, vol. 16, no. 5, pp. 490–495, 1948.

[32] E. Worch, *Adsorption Technology in Water Treatment, Fundamentals, Processes, and Modeling*, Walter de Gruyter, Berlin, Germany, 2012.

[33] C. J. Geankoplis, *Procesos de transporte y operaciones unitarias*, Compañía Editorial Continental, México, 3rd edition, 1998.

[34] H. C. Thomas, "Heterogeneous ion exchange in a flowing system," *Journal of the American Chemical Society*, vol. 66, no. 10, pp. 1664–1666, 1944.

[35] Y. H. Yoon and J. H. Nelson, "Application of gas adsorption kinetics I. A theoretical model for respirator cartridge service life," *American Industrial Hygiene Association Journal*, vol. 45, no. 8, pp. 509–516, 1984.

[36] R. M. Clark, "Evaluating the cost and performance of field-scale granular activated carbon systems," *Environmental Science & Technology*, vol. 21, no. 6, pp. 573–580, 1987.

[37] G. Yan and T. Viraraghavan, "Heavy metal removal in a biosorption column by immobilized M. rouxii biomass," *Bioresource Technology*, vol. 78, no. 3, pp. 243–249, 2001.

[38] G. S. Bohart and E. Q. Adams, "Some aspects of the behavior of charcoal with respect to chlorine," *Journal of the American Chemical Society*, vol. 42, no. 3, pp. 523–544, 1920.

[39] Y. Liu, "Is the free energy change of adsorption correctly calculated?" *Journal of Chemical & Engineering Data*, vol. 54, no. 7, pp. 1981–1985, 2009.

[40] J. Kielland, "Individual activity coefficients of ions in aqueous solutions," *Journal of the American Chemical Society*, vol. 59, no. 9, pp. 1675–1678, 1937.

[41] R. A. Fideles, G. M. D. Ferreira, F. S. Teodoro et al., "Trimellitated sugarcane bagasse: a versatile adsorbent for removal of cationic dyes from aqueous solution. Part I: batch adsorption in a monocomponent system," *Journal of Colloid and Interface Science*, vol. 515, pp. 172–188, 2018.

[42] O. Karnitz, L. V. A. Gurgel, R. P. de Freitas, and L. F. Gil, "Adsorption of Cu(II), Cd(II), and Pb(II) from aqueous single metal solutions by mercerized cellulose and mercerized sugarcane bagasse chemically modified with EDTA dianhydride (EDTAD)," *Carbohydrate Polymers*, vol. 77, no. 3, pp. 643–650, 2009.

[43] L. V. A. Gurgel, R. P. de Freitas, and L. F. Gil, "Adsorption of Cu(II), Cd(II), and Pb(II) from aqueous single metal solutions by sugarcane bagasse and mercerized sugarcane bagasse chemically modified with succinic anhydride," *Carbohydrate Polymers*, vol. 74, no. 4, pp. 922–929, 2008.

[44] O. KarnitzJr., L. V. A. Gurgel, J. C. P. de Melo et al., "Adsorption of heavy metal ion from aqueous single metal solution by chemically modified sugarcane bagasse," *Bioresource Technology*, vol. 98, no. 6, pp. 1291–1297, 2007.

[45] M. M. C. Elias, G. M. D. Ferreira, F. T. R. de Almeida et al., "Synthesis and application of sugarcane bagasse cellulose mixed esters. Part I: removal of Co^{2+} and Ni^{2+} from single spiked

aqueous solutions in batch mode using sugarcane bagasse cellulose succinate phthalate," *Journal of Colloid and Interface Science*, vol. 533, pp. 678–691, 2019.

[46] O. Karnitz, L. V. A. Gurgel, and L. F. Gil, "Removal of Ca(II) and Mg(II) from aqueous single metal solutions by mercerized cellulose and mercerized sugarcane bagasse grafted with EDTA dianhydride (EDTAD)," *Carbohydrate Polymers*, vol. 79, no. 1, pp. 184–191, 2010.

[47] K. A. G. Gusmao, L. V. A. Gurgel, T. M. S. Melo, and L. F. Gil, "Application of succinylated sugarcane bagasse as adsorbent to remove methylene blue and gentian violet from aqueous solutions—kinetic and equilibrium studies," *Dyes and Pigments*, vol. 92, no. 3, pp. 967–974, 2012.

[48] B. H. Hameed, I. A. W. Tan, and A. L. Ahmad, "Adsorption isotherm, kinetic modeling and mechanism of 2,4,6-trichlorophenol on coconut husk-based activated carbon," *Chemical Engineering Journal*, vol. 144, no. 2, pp. 235–244, 2008.

[49] C. H. Giles, D. Smith, and A. Huitson, "A general treatment and classification of the solute adsorption isotherm. I. Theoretical," *Journal of Colloid and Interface Science*, vol. 47, pp. 755–765, 1974.

[50] B. C. S. Ferreira, F. S. Teodoro, A. B. Mageste, L. F. Gil, R. P. de Freitas, and L. V. A. Gurgel, "Application of a new carboxylate-functionalized sugarcane bagasse for adsorptive removal of crystal violet from aqueous solution: kinetic, equilibrium and thermodynamic studies," *Industrial Crops and Products*, vol. 65, pp. 521–534, 2015.

[51] R. A. Ogwada and D. L. Sparks, "Kinetics of ion exchange on clay minerals and soil: II. Elucidation of rate-limiting steps," *Soil Science Society of America Journal*, vol. 50, no. 5, pp. 1162–1166, 1986.

[52] B. Volesky, "Biosorption process simulation tools," *Hydrometallurgy*, vol. 71, no. 1–2, pp. 179–190, 2003.

[53] A.B. de Haan, *Process technology: an introduction*, Walter de Gruyter, Berlin, Germany, 2015.

[54] J.-D. Chen, J.-X. Yu, F. Wang et al., "Selective adsorption and recycle of Cu^{2+} from aqueous solution by modified sugarcane bagasse under dynamic condition," *Environmental Science and Pollution Research*, vol. 24, no. 10, pp. 9202–9209, 2017.

[55] H.-P. Chao, C.-C. Chang, and A. Nieva, "Biosorption of heavy metals on *Citrus maxima* peel, passion fruit shell, and sugarcane bagasse in a fixed-bed column," *Journal of Industrial and Engineering Chemistry*, vol. 20, no. 5, pp. 3408–3414, 2014.

[56] A. Abdolali, H. H. Ngo, W. Guo et al., "Application of a breakthrough biosorbent for removing heavy metals from synthetic and real wastewaters in a lab-scale continuous fixed-bed column," *Bioresource Technology*, vol. 229, pp. 78–87, 2017.

[57] B. A. Shah, C. B. Mistry, and A. V. Shah, "Sequestration of Cu(II) and Ni(II) from wastewater by synthesized zeolitic materials: equilibrium, kinetics and column dynamics," *Chemical Engineering Journal*, vol. 220, pp. 172–184, 2013.

[58] M. Kapur and M. K. Mondal, "Design and model parameters estimation for fixed–bed column adsorption of Cu(II) and Ni(II) ions using magnetized saw dust," *Desalination and Water Treatment*, vol. 57, no. 26, pp. 12192–12203, 2016.

[59] K. Vijayaraghavan, J. Jegan, K. Palanivelu, and M. Velan, "Biosorption of cobalt(II) and nickel(II) by seaweeds: batch and column studies," *Separation and Purification Technology*, vol. 44, no. 1, pp. 53–59, 2005.

[60] M. Galedar and H. Younesi, "Biosorption of ternary cadmium, nickel and cobalt ions from aqueous solution onto *Saccharomyces cerevisiae* cells: batch and column studies," *American Journal of Biochemistry and Biotechnology*, vol. 9, no. 1, pp. 47–60, 2013.

[61] B. Li, F. Liu, J. Wang et al., "Efficient separation and high selectivity for nickel from cobalt-solution by a novel chelating resin: batch, column and competition investigation," *Chemical Engineering Journal*, vol. 195–196, pp. 31–39, 2012.

[62] S. Vilvanathan and S. Shanthakumar, "Column adsorption studies on nickel and cobalt removal from aqueous solution using native and biochar form of *Tectona grandis*," *Environmental Progress & Sustainable Energy*, vol. 36, no. 4, pp. 1030–1038, 2017.

[63] C. E. R. Barquilha, E. S. Cossich, C. R. G. Tavares, and E. A. Silva, "Biosorption of nickel(II) and copper(II) ions in batch and fixed-bed columns by free and immobilized marine algae *Sargassum* sp," *Journal of Cleaner Production*, vol. 150, pp. 58–64, 2017.

[64] C. E. Borba, E. A. da Silva, M. R. Fagundes-Klen, A. D. Kroumov, and R. Guirardello, "Prediction of the copper (II) ions dynamic removal from a medium by using mathematical models with analytical solution," *Journal of Hazardous Materials*, vol. 152, no. 1, pp. 366–372, 2008.